Int. J. Heat Mass Transfer. Vol. 36, No. 15, pp. 3773–3782, 1993
Printed in Great Britain

0017–9310/93 $6.00 + 0.00

Double-diffusive convection in a rotating annulus with horizontal temperature and vertical solutal gradients

HYUNG JIN SUNG,† WON KOOK CHO and JAE MIN HYUN
Department of Mechanical Engineering, Korea Advanced Institute of Science and Technology, Yusong, Taejon, 305-701, South Korea

(*Received* 29 *October* 1992 *and in final form* 25 *February* 1993)

Abstract—A numerical study is made of double-diffusive convection in a rotating annulus. Motions are driven by the externally applied horizontal temperature gradient. The stable solutal gradient is aligned in the vertical direction. Parametric studies are performed in order to acquire an understanding of the qualitative character of the axisymmetric basic state of the resulting flow. The aim is to inquire as to the effect of rotation on the global flow structure. A high-accuracy pseudospectral numerical scheme is employed to integrate the axisymmetric incompressible Navier–Stokes equations. Computational results are presented to disclose the detailed fields of azimuthal and meridional flows, temperature, and solute. A total of nine parameter sets, produced by a combination of three values of stratification number and three buoyancy ratios, were dealt with in the computation. The Prandtl number was set $Pr = 1.0$, the thermal Rayleigh number $Ra_T = 10^5$, and the Lewis number $Le = 10.0$. For a low buoyancy ratio, motions are vigorous, especially when the rotation effect is small, resembling a sidewall-heated pure thermal convection. In the interior, a linear temperature stratification and a well-mixed solutal field are seen. When the buoyancy ratio is moderate, the overall character of flow shows considerable dependence on the relative strength of rotation effect. For a large buoyancy ratio, the stabilizing solutal effect is dominant. The convective activities are very weak, and heat transfer is mostly conductive.

1. INTRODUCTION

BUOYANCY-DRIVEN motions of a fluid, due to the simultaneous presence of two (or possibly more) diffusive components, are generally termed double-diffusive convection [1]. This type of convection has long been recognized to be significant, among others, in oceanic flow processes. For the oceans, the primary diffusing agents are heat and concentration of matter (e.g. salt). A substantial amount of research has been accumulated on this topic [2, 3].

Recent advances in material processing technologies have expanded the interests in double-diffusive convective transport phenomena. In these situations, double-diffusive convection is caused by the gradients of temperature and of solute (e.g. dopant or impurity) in the flow field. In response to the developments in engineering applications, considerable effort has been devoted to the study of double-diffusive convection in a confined space. Of particular interest is the flow configuration, in which the external temperature gradient is imposed in the horizontal and the solutal gradient in the vertical direction [4]. This flow geometry provides a rudimentary model for the growth of crystals [5]. Some of the fundamental flow characteristics of this double-diffusive convection in a rectangular cavity of aspect ratio $O(1)$ have been demonstrated by experimental visualizations as well as numerical simulations [6–12]. These preceding findings, although restricted in scope and in parameter settings, established the major dimensionless parameters and identified some of the distinctive flow regimes. Especially, the layered velocity field structure and the associated thermal and solutal fields were delineated by detailed numerical simulations [4].

It should be pointed out that, in many practical situations of material processing engineering applications, the entire system rotates steadily about a vertical axis [5]. The rotation is intended to provide an additional means of control of the whole dynamic system. It then follows that the dynamics of flow is crucially influenced by the rotation effects. These concerns warrant in-depth evaluations of transport phenomena in more realistic situations pertinent to modern material processing procedures.

In this paper, a systematic numerical investigation was conducted of double-diffusive convection in a closed, rotating annular cavity. Attention is directed to the flow configurations which give rise to double-diffusive convective motions under reasonably strong rotation effects. In the present work, therefore, numerical solutions are sought to depict the axisymmetric flows attainable in cylindrical geometries. Parametric studies were performed to reveal the impacts of principal dynamic ingredients involved in the processes. By the introduction of rotation effects, the system also entails, in addition to the usual forces, the

† Author to whom correspondence should be addressed.

NOMENCLATURE

D	diameter
g	gravitational acceleration
H	depth of annulus
Le	Lewis number, κ/κ_S
N	Brunt–Vaisala frequency, $\sqrt{(\alpha_S g \Delta S/H)}$
p	reduced pressure
Pr	Prandtl number, ν/κ
r	radial space coordinate
Ra_S	solutal Rayleigh number, $g\alpha_S \Delta S H^3/\kappa_S \nu$
Ra_T	thermal Rayleigh number, $g\alpha_T \Delta T H^3/\kappa\nu$
R_ρ	buoyancy ratio, Ra_S/Ra_T
S	solute concentration
St	stratification parameter $(N/\Omega)^2$
T	temperature
t	time coordinate
u	radial velocity component
v	azimuthal velocity component in a rotating frame
w	axial velocity component
z	axial space coordinate.

Greek symbols

α_T	coefficient of thermal expansion
α_S	solute analogue, α_T
β_T	thermal Rossby number, $\alpha_T g \Delta T/4\Omega^2 H$
β_S	solutal Rossby number, $\alpha_S g \Delta S/4\Omega^2 H$
ε	Ekman number, $\nu/2\Omega H^2$
η	azimuthal vorticity component
κ	thermal diffusivity
κ_S	solutal diffusivity
ν	kinematic viscosity
ρ	density
Ψ	meridional stream function
Ω	local angular velocity.

Superscript

*	dimensional variables.

Coriolis force, centrifugal force, and the curvature effects in the overall force balance. The present study, therefore, may be construed as being a sequel to the earlier numerical accounts [4], which dealt with double-diffusive convection in a non-rotating environment.

The numerically constructed axisymmetric flows will provide source information against which future experimental data could be compared. Furthermore, the computed axisymmetric flows will serve as the basic states to analyze complex three-dimensional flows which are possible under proper parameters spaces.

2. NUMERICAL MODEL

Consider a viscous incompressible fluid, of kinematic viscosity ν, thermal diffusivity κ_T, and solutal diffusivity κ_S, contained in a vertically mounted cylindrical annulus of height H, and the radius of the inner (outer) sidewall is H ($2H$) (i.e. the aspect ratio, height/width is 1.0). In accordance with the basic problem statement, double-diffusive convection is maintained by the interplay of the externally applied temperature gradient (in the horizontal direction) and the solutal gradient (in the vertical direction). The entire setup is placed on a rotating turntable, which rotates steadily at angular frequency Ω about the annulus central axis. The task is to describe the axisymmetric flow in the rotating annulus, and a schema is shown in Fig. 1.

The fluid flow is governed by the Navier–Stokes equations, and the Boussinesq-fluid approximation will be incorporated. Viewed in a rotating cylindrical coordinate system (r, θ, z), with the corresponding velocity components (u, v, w), these equations can be expressed as

$$\frac{\partial u}{\partial t} = -\frac{\partial}{r\,\partial r}(ru^2) - \frac{\partial}{\partial z}(uw) + \left(1+\frac{v}{r}\right)v - \frac{\partial p}{\partial r} + \varepsilon\left(\nabla^2 u - \frac{u}{r^2}\right) \quad (1)$$

$$\frac{\partial v}{\partial t} = -\frac{\partial}{r\,\partial r}(ruv) - \frac{\partial}{\partial z}(vw) - \left(1+\frac{v}{r}\right)u + \varepsilon\left(\nabla^2 v - \frac{v}{r^2}\right) \quad (2)$$

$$\frac{\partial w}{\partial t} = -\frac{\partial}{r\,\partial r}(ruw) - \frac{\partial}{\partial z}(w^2) - \frac{\partial p}{\partial z} + \beta_T T - \beta_S S + \varepsilon\nabla^2 w \quad (3)$$

$$\frac{\partial T}{\partial t} = -\frac{\partial}{r\,\partial r}(ruT) - \frac{\partial}{\partial z}(wT) + \frac{\varepsilon}{Pr}\nabla^2 T \quad (4)$$

$$\frac{\partial S}{\partial t} = -\frac{\partial}{r\,\partial r}(ruS) - \frac{\partial}{\partial z}(wS) + \frac{\varepsilon}{Pr\,Le}\nabla^2 S \quad (5)$$

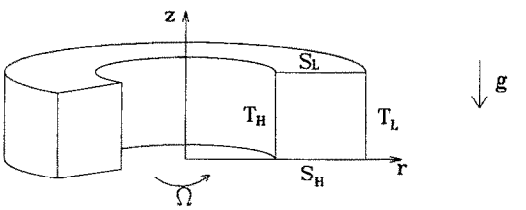

FIG. 1. Schematic diagram of the model.

$$\frac{\partial}{r\,\partial r}(ru)+\frac{\partial w}{\partial z}=0 \tag{6}$$

$$\rho=\rho_0[1-\alpha_T(T-T_0)+\alpha_S(S-S_0)] \tag{7}$$

where

$$\nabla^2=\frac{\partial}{r\,\partial r}\left(r\frac{\partial}{\partial r}\right)+\frac{\partial^2}{\partial z^2}.$$

The coefficient of thermometric (solutal) expansion of the fluid is noted by $\alpha_T(\alpha_S)$.

In the above, the equations have been made dimensionless by adopting the following non-dimensional quantities: $(r,z)=(r^*,z^*)/H$, $t=t^*(2\Omega)$, $V=V^*/2H\Omega$, $S=(S^*-S_0^*)/\Delta S$, $T=(T^*-T_0^*)/\Delta T$, $p=p^*/(\rho_0^*4\Omega^2H^2)$, $\rho=\rho^*/\rho_0^*$, in which the asterisk denotes the dimensional counterparts. The externally imposed dimensional temperature (solute) difference across the annulus width (height) is $\Delta T(\Delta S)$, and subscript 0 indicates the reference value.

As is obvious in the governing equations, the following relevant non-dimensional parameters emerge:

$\varepsilon=\dfrac{\nu}{2\Omega H^2}$, Ekman number

$Ra_T=\dfrac{g\alpha_T\Delta TH^3}{\kappa_T\nu}$, thermal Rayleigh number

$Ra_S=\dfrac{g\alpha_S\Delta SH^3}{\kappa_S\nu}$, solutal Rayleigh number

$R_\rho=\dfrac{Ra_S}{Ra_T}$, buoyancy ratio

$Pr=\dfrac{\nu}{\kappa_T}$, Prandtl number

$Le=\dfrac{\kappa_T}{\kappa_S}$, Lewis number

$N=\sqrt{\left(\dfrac{\alpha_S g\Delta S}{H}\right)}$, Brunt–Vaisala frequency

$St=\left(\dfrac{N}{\Omega}\right)^2$, stratification parameter

$\beta_T=\alpha_T g\Delta T/4\Omega^2H$, thermal Rossby number

$\beta_S=\alpha_S g\Delta S/4\Omega^2H$, solutal Rossby number.

The unsteady terms are retained for the purpose of numerical calculations, and the large-time converged solutions will be taken as the steady state values. In the actual numerical model, the fluid is initially in a state of rigid-body rotation at uniform temperature $T=0$ everywhere, with a vertically linear solutal distribution. At time $t=0$, the temperature at the inner cylindrical side wall ($r=1$) is raised to $T=1$ and maintained so thereafter. The horizontal lids are thermally insulated, and the vertical side walls are impermeable to solute. Viewed in the frame rotating at Ω, the velocity components are zero at the solid walls. Therefore, the initial and boundary conditions are written as

$$T=0,\quad \frac{\partial S}{\partial z}=\frac{\Delta S}{H},\quad u=v=w=0,\quad \text{at } t=0 \tag{8}$$

and

$$\frac{\partial T}{\partial z}=0,\quad S=1,\quad u=v=w=0,\quad \text{at } z=0$$

$$\frac{\partial T}{\partial z}=0,\quad S=0,\quad u=v=w=0,\quad \text{at } z=1$$

$$T=1,\quad \frac{\partial S}{\partial z}=0,\quad u=v=w=0,\quad \text{at } r=1$$

$$T=0,\quad \frac{\partial S}{\partial z}=0,\quad u=v=w=0,\quad \text{at } r=2. \tag{9}$$

The above system of equations is solved by adopting a numerical scheme based on a high-accuracy pseudo-spectral method. In the azimuthal direction, the Fourier series is employed as the expansion function. In the radial and vertical directions, the Chebyshev polynomials are used. The method of matrix multipliers is utilized to evaluate the first and second derivatives. The unsteady solutions are acquired, using the time-splitting technique of Chorin [13]. The crux of this numerical procedure is that all the calculations can be conveniently represented in the form of matrix operators. Consequently, the main parts of the routine are fully vectorized for the modern supercomputer with vector processors. The details of the present numerical schemes are available in Ku *et al.* [14, 15]; by implementing an amended version of this numerical method, Hyun and Kwak [9] recently reported a successful depiction of three-dimensional baroclinic waves in a rotating annulus. The calculations in the present study were made on a CRAY-YMP supercomputer.

3. RESULTS AND DISCUSSION

A large number of non-dimensional parameters are involved in the flow processes. It is, therefore, essential that the parametric studies should be carefully sorted out, such that the principal parameter spaces are to be properly covered. The major objective of the present study is to comprehend the qualitative effect of the rotation of the cavity on the character of double-diffusive convection in the container. Accordingly, the characteristic variations of St, denoting the relative strengths of buoyancy and rotation, were given due consideration. In the present computations, three decades of the values of St, i.e. 0.1, 1.0, and 10.0, were selected. These would exemplify the situations whereby the rotation effect, compared to the overall buoyancy effect, is dominant, comparable, and minor, respectively. Another crucial parameter in double-diffusive convection is the buoyancy ratio R_ρ; this was amply stressed in the prior studies for non-rotating

double-diffusion [16, 17]. The eminent character of flow is determined by the interplay of buoyancy effects due to the temperature and solutal gradients. Consequently, three values of $R_\rho(=0.1, 1.0, 10.0)$ were chosen for computations. Again, these would span the characteristic parameter regions whereby the stabilizing solutal effect is, respectively, meager, comparable, and dominant in comparison to the destabilizing temperature effect. In line with this reasoning, a total of nine sets of explicit computational results were obtained. The Prandtl number was set as $Pr = 1.0$, the thermal Rayleigh number $Ra_T = 10^5$, and the Lewis number $Le = 10.0$. In the present formulations, the values of the Ekman number cannot be independently prescribed once these other parameters are fixed. For all the computed cases, however, the Ekman numbers are always much smaller than unity.

The results are now examined in a systematic manner to disclose the main character of flow. For each computational set, four plots are constructed to illustrate the isolines of azimuthal velocity (v), meridional stream function (Ψ), temperature (T), and solutal (S) fields. Here, Ψ is defined such that $u = \partial\Psi/r\,\partial r$, $w = -(\partial\Psi/r\,\partial r)$ [9].

Much can also be learned about the relative importance of the individual dynamical effect which are expressed in the governing equations. For this purpose, the equation for the azimuthal vorticity, $\eta = (\partial u/\partial z) - (\partial w/\partial r)$, is useful. This equation can be obtained by cross-differentiating the u- and w-momentum equations

$$\frac{\partial \eta}{\partial t} = \underbrace{-u\left(\frac{\partial \eta}{\partial r} - \frac{\eta}{r}\right)}_{(A)} \underbrace{-w\frac{\partial \eta}{\partial z} + \left(1 + \frac{v}{r}\right)\frac{\partial v}{\partial r}}_{(B)} + \varepsilon\underbrace{\left[\frac{\partial}{\partial r}\left(\frac{\partial r\eta}{\partial r}\right) + \frac{\partial^2 \eta}{\partial z^2}\right]}_{(C)} \underbrace{-\beta_T\frac{\partial T}{\partial r}}_{(D)} + \underbrace{\beta_S\frac{\partial S}{\partial r}}_{(E)}. \quad (10)$$

The marked terms on the right-hand side of equation (10) represent, respectively, the nonlinear advection (A), Coriolis and curvature effects (B), viscous diffusion effect (C), buoyancy due to temperature gradient (D), and buoyancy due to solutal gradient (E). The relative magnitudes of these terms will be compared in an effort to gauge the significance of each dynamic effect.

The results pertaining to the case of $R_\rho = 0.1$ are exhibited in Figs. 2–4. In accordance with the definition of R_ρ, the thermal buoyancy effect outweighs the solutal buoyancy effect. It is recalled that, in the present flow setup, the horizontally directed thermal gradient is the primary cause for convective motions. The stable solutal gradient, which is aligned in the vertical, tends to inhibit vertical flows. Figure 2(a) exemplifies the case of small St ($St = 0.1$, and for this parameter set, the Ekman number $\varepsilon = 1.85 \times 10^{-3}$). The comparative influence of rotation effect is substantial. The meridional circulation flows and the associated azimuthal flow are moderate in magnitude. The azimuthal velocity is positive (negative) in the lower (upper) portion of the cavity. The isotherms in

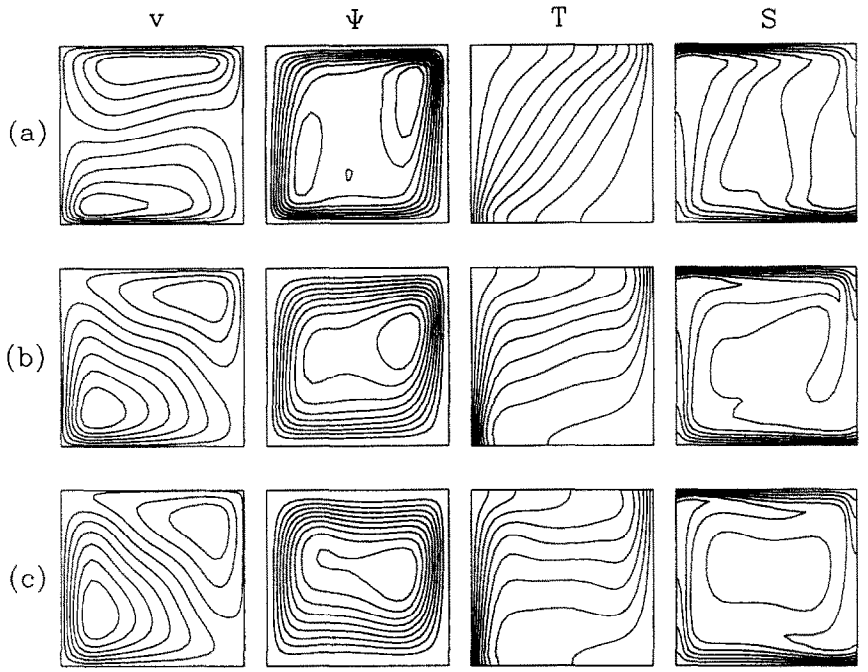

FIG. 2. Contour plots of azimuthal velocity (v), meridional stream function (Ψ), isotherms (T) and isosolutal lines (S). $R_\rho = 0.1$. (a) $St = 0.1$; $|v|_{max} = 1.0 \times 10^{-1}$, $|\Psi|_{max} = 5.8 \times 10^{-3}$; (b) $St = 1.0$: $|v|_{max} = 4.6 \times 10^{-1}$, $|\Psi|_{max} = 5.4 \times 10^{-2}$; (c) $St = 10.0$: $|v|_{max} = 5.9 \times 10^{-1}$, $|\Psi|_{max} = 2.2 \times 10^{-1}$.

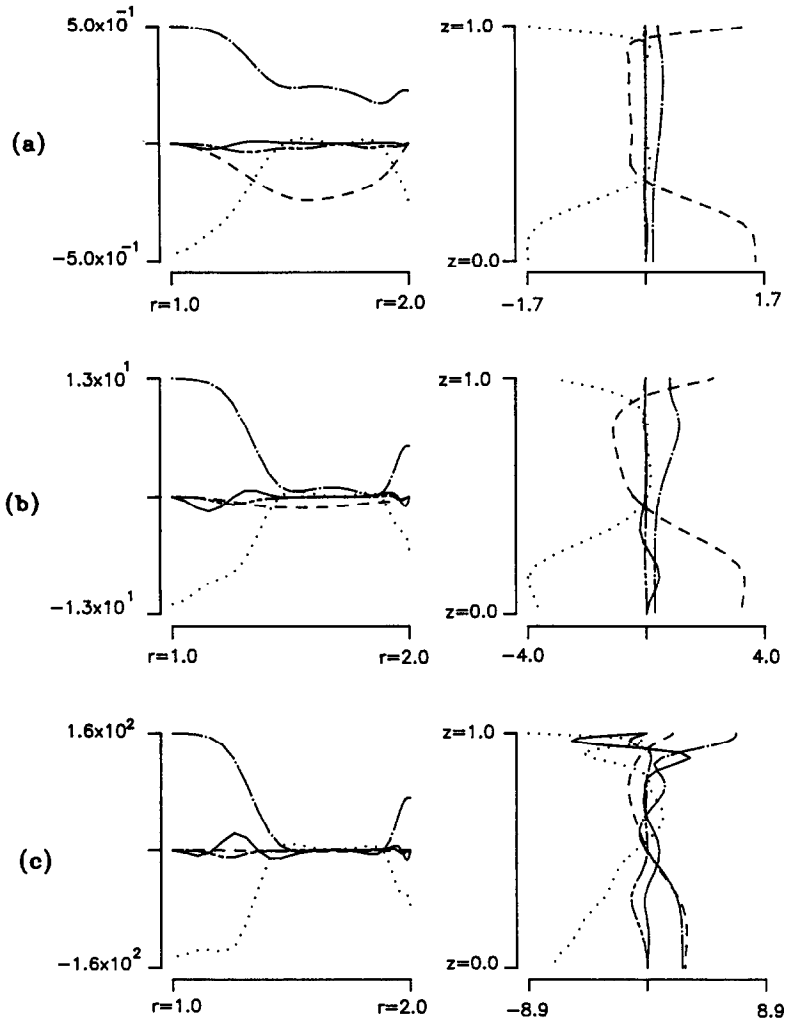

FIG. 3. Comparisons of the relative magnitudes of the terms in the vorticity equation (10). $R_\rho = 0.1$: (a) $St = 0.1$, (b) $St = 1.0$, (c) $St = 10.0$. ——: nonlinear advection term (A); – – – –: vertical shear of azimuthal velocity (B); · · · · ·: viscous term (C); — · — · — · —: horizontal temperature gradient (D); — — — — — —: horizontal solute gradient (E).

the interior are generally tilted from the lower side of the inner sidewall to the upper side of the outer sidewall. As is discernible in Fig. 3(a), in the interior region closer to the outer sidewall, the dominant balance is between the vertical shear of azimuthal velocity (term (B) in equation (10)) and the horizontal gradient of temperature (term (D) in equation (10)). This is a manifestation of the well-known thermal wind relation. The stratification of the solutal field is mostly confined to the zones adjacent to the horizontal endwalls. In the middle portion of the cavity, due to the convective activities, the solutal field has been fairly homogeneous. The profile of the Nusselt number at the inner sidewall $Nu|_{r=1}$ shows a generally decreasing pattern with height; this reflects the cluster of isotherms near the bottom portion of the inner sidewall.

As the stratification number St increases, the relative importance of the rotation decreases. Consequently, the convective activities, driven by the horizontally applied temperature gradient, intensify. The isotherms in the interior core exhibit the tendency of a horizontal alignment, suggesting an approach to a linear temperature stratification. As a result of these intense convective motions, the Nusselt number at the inner sidewall takes a larger value, in particular, near the bottom part of the inner sidewall. When St is large (see Fig. 2(c) for $St = 10.0$), the rotation effect is minor, and the global flow structure resembles that of a sidewall-heated thermal convection in a nonrotating environment. It should be mentioned here that, in the present formulation, the value of ε increases with increasing St. Therefore, for the example treated in Fig. 2(c), appreciable viscous effects are also felt throughout the flow field.

The results for $R_\rho = 1.0$ are illustrated in Figs. 5–7. The effect of the flow-driving horizontal temperature gradient is comparable to the effect of the stable solu-

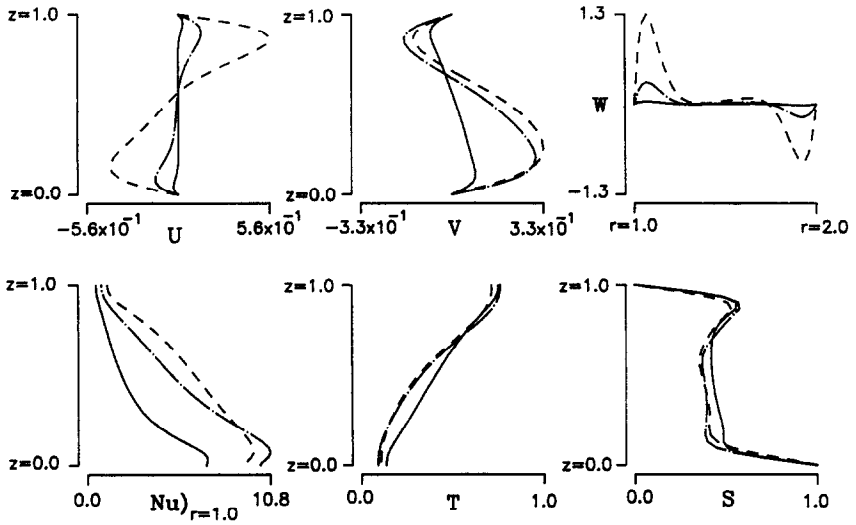

FIG. 4. Representative profiles of velocities, Nusselt number, temperature and solute. $R_\rho = 0.1$. The vertical profiles are along $r = 0.5$, and the horizontal profiles are along $z = 0.5$. ——: $St = 0.1$, — · — · — · —: $St = 1.0$, – – – –: $St = 10.0$.

tal gradient. It is readily seen in Figs. 5–7 that the convective activities are generally weaker than for $R_\rho = 0.1$ (note the difference in magnitudes of $|v|_{max}$ and $|\Psi|_{max}$ between Fig. 5 and Fig. 2). When St is small, as demonstrated in Fig. 5(a), due to the overriding rotation effect, the convective velocities weaken considerably. Much of the meridional circulation is confined to the areas adjacent to the solid surfaces. The isotherms are almost parallel and vertical. This implies that heat transfer is dominated by conductive mode. The Nusselt number at the inner sidewall, therefore, is rather small and is fairly uniform with height. The iso-solutal lines in the interior are tilted from the upper portion of the inner sidewall to the lower portion of the outer sidewall. The tilting of the iso-solutal lines reflects the presence of weak convective motions in the interior.

The profiles of the individual terms of equation (10)

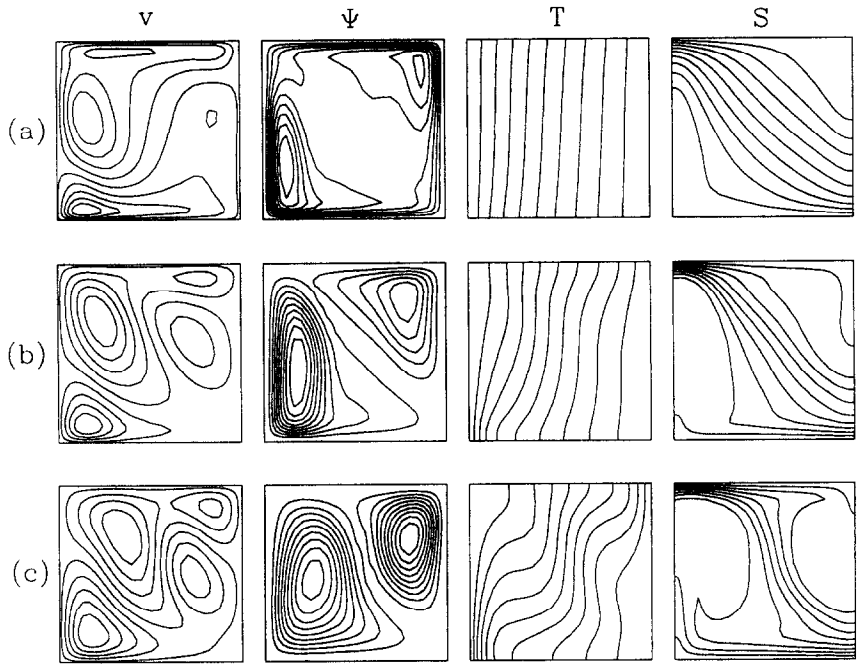

FIG. 5. Contour plots of azimuthal velocity (v), meridional stream function (Ψ), isotherms (T) and iso-solutal lines (S). $R_\rho = 1.0$. (a) $St = 0.1$: $|v|_{max} = 4.9 \times 10^{-3}$, $|\Psi|_{max} = 1.6 \times 10^{-4}$; (b) $St = 1.0$: $|v|_{max} = 5.8 \times 10^{-2}$, $|\Psi|_{max} = 3.5 \times 10^{-3}$; (c) $St = 10.0$: $|v|_{max} = 1.6 \times 10^{-1}$, $|\Psi|_{max} = 3.1 \times 10^{-2}$.

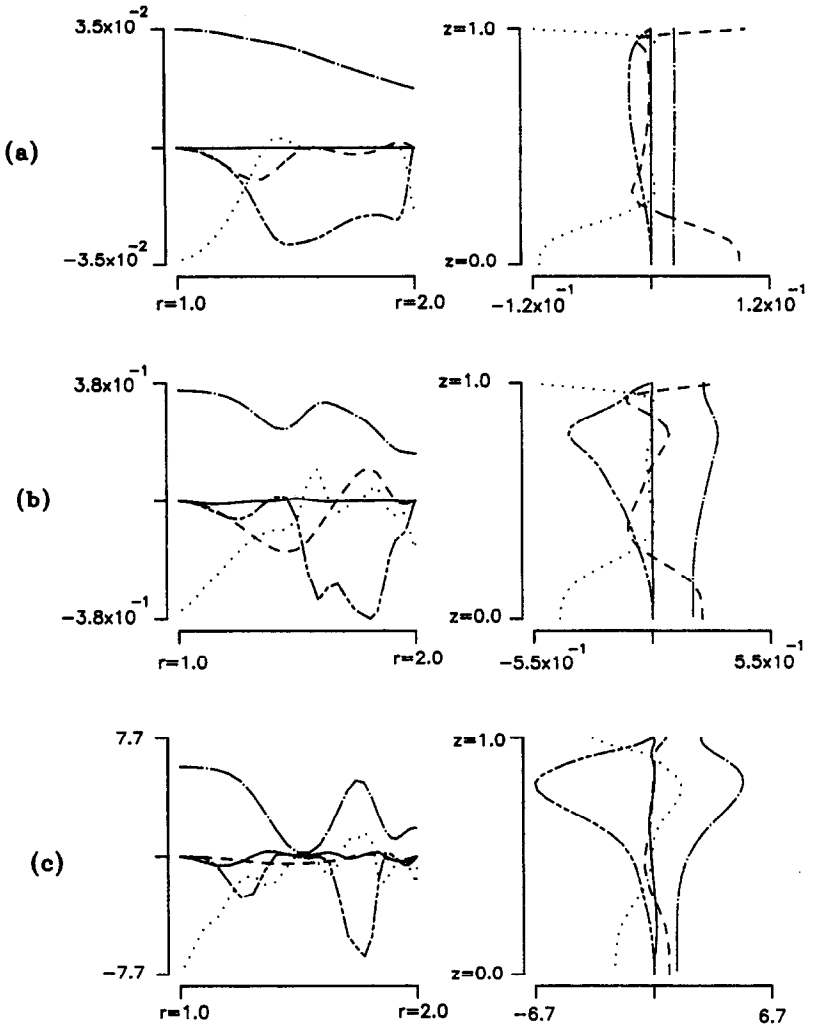

FIG. 6. Comparisons of the relative magnitudes of the terms in the vorticity equation (10). $R_\rho = 1.0$: (a) $St = 0.1$, (b) $St = 1.0$, (c) $St = 10.0$. ——: nonlinear advection term (A); – – – –: vertical shear of azimuthal velocity (B); · · · · ·: viscous term (C); — · — · — · —: horizontal temperature gradient (D); — — — — — —: horizontal solute gradient (E).

are also revealing. The most notable dynamical ingredients for $R_\rho = 1.0$ in the bulk of interior away from the inner sidewall are generally the thermal and solutal buoyancy terms. As the rotation effect becomes small, such terms as the Coriolis force (denoted by term (B) in equation (10)) weaken in magnitude. Therefore, the overall balance is maintained by the two opposing buoyancy effects, and these observations are consistent with the computed results demonstrated in Figs. 5–7. As St increases, the relative influence of the rotational constraint diminishes, and the global convective activities due to the thermal gradient strengthen accordingly. The tendency toward the horizontally aligned isotherms in the interior is evident in Fig. 5(c). The heat transfer is augmented by these vigorous convective motions, as displayed in Fig. 7. It is noticed here again that, as St increases, the value of ε also increases in the present problem setup. The meridional circulations, as illustrated in Fig. 5(c), are quite diffused and they fill much of the bulk of the interior. The solutal field in the interior generally increases rather monotonically with height. As St increases, the variations of S become somewhat steeper in the regions closer to the horizontal endwalls.

Finally, the computed results for $R_\rho = 10.0$ are depicted in Figs. 8–10. The effect of the stable solutal gradient dominates the flow-driving effect of horizontal temperature gradient. As anticipated, the convective activities are suppressed, and the heat transfer is controlled mostly by conduction. The isotherms are nearly parallel and vertical. The linearly stratified solutal field remains substantially undisturbed. The consequence of the largely conductive heat transfer turns up in the plots of $Nu|_{r=1}$. The Nusselt number at the inner sidewall is very small and is almost uniform with height. As depicted in Fig. 9, the prominent dynamical effects are represented by the two opposing

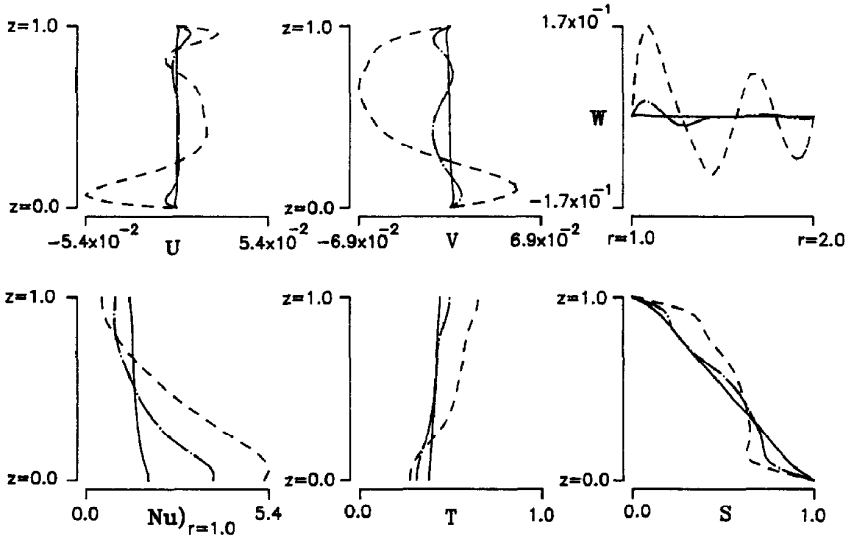

FIG. 7. Representative profiles of velocities, Nusselt number, temperature and solute. $R_\rho = 1.0$. The vertical profiles are along $r = 0.5$, and the horizontal profiles are along $z = 0.5$. ——: $St = 0.1$, — · — · —: $St = 1.0$, – – –: $St = 10.0$.

buoyancy terms (terms (D) and (E) in equation (10)). It is stressed in Fig. 8 that both the azimuthal and meridional flows are extremely small in magnitude (note the orders of magnitudes of the values of $|v|_{max}$ and $|\Psi|_{max}$). In particular, when St is small, the concentration of the meridional flows to narrow zones adjacent to the solid walls is notable. Both the profiles of u and w, as shown in Fig. 10, indicate that, in the bulk of the interior, virtually no meridional flows are discernible.

4. CONCLUSION

The computational results disclose the prominent features of axisymmetric double-diffusive convection in a rotating annulus. The objective is to depict the

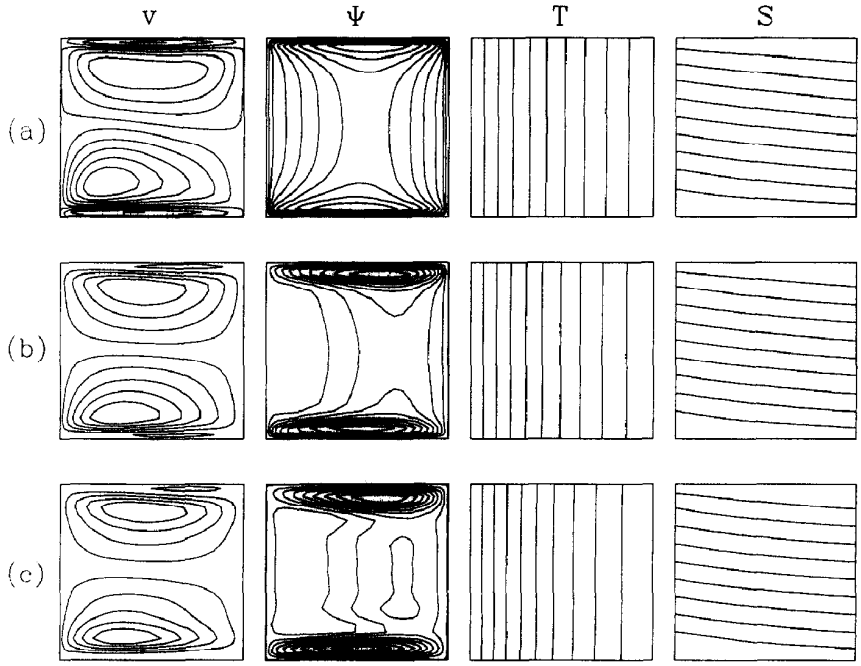

FIG. 8. Contour plots of azimuthal velocity (v), meridional stream function (Ψ), isotherms (T) and isosolutal lines (S). $R_\rho = 10.0$. (a) $St = 0.1$: $|v|_{max} = 9.6 \times 10^{-5}$, $|\Psi|_{max} = 1.3 \times 10^{-6}$; (b) $St = 1.0$: $|v|_{max} = 5.8 \times 10^{-4}$, $|\Psi|_{max} = 1.0 \times 10^{-5}$; (c) $St = 10.0$: $|v|_{max} = 1.4 \times 10^{-3}$, $|\Psi|_{max} = 6.3 \times 10^{-5}$.

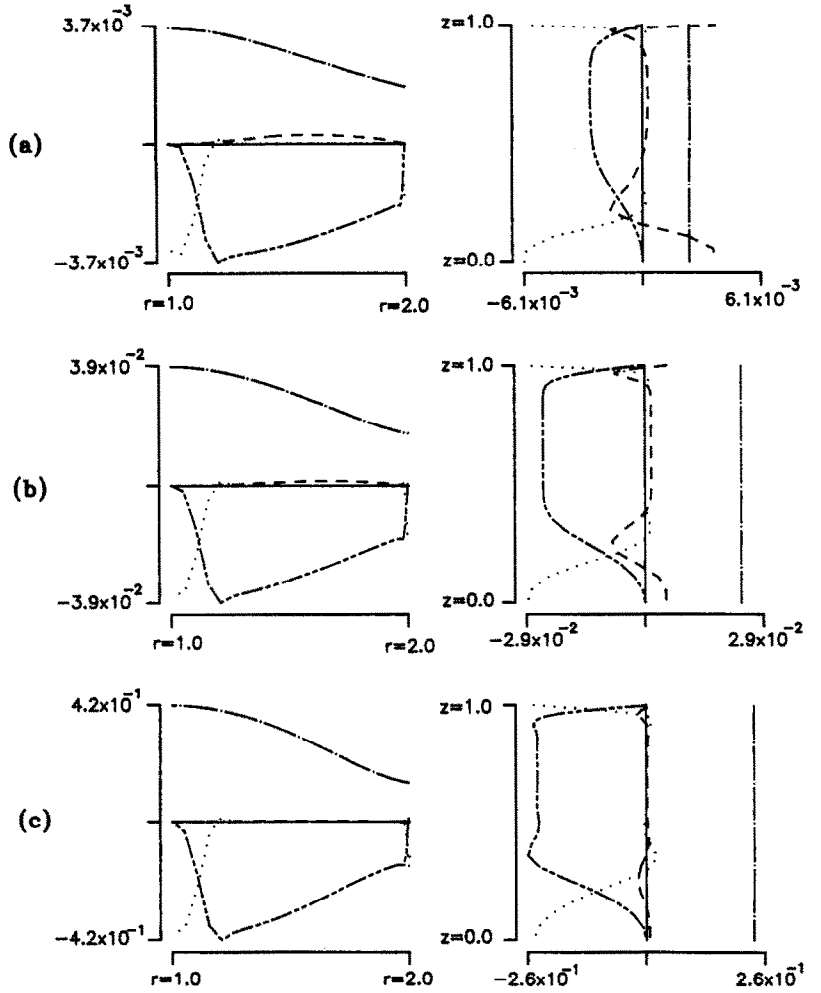

FIG. 9. Comparisons of the relative magnitudes of the terms in the vorticity equation (10). $R_\rho = 10.0$: (a) $St = 0.1$, (b) $St = 1.0$, (c) $St = 10.0$. ——: nonlinear advection term (A); – – – –: vertical shear of azimuthal velocity (B); · · · · ·: viscous term (C); — · — · — · —: horizontal temperature gradient (D); — — — — — —: horizontal solute gradient (E).

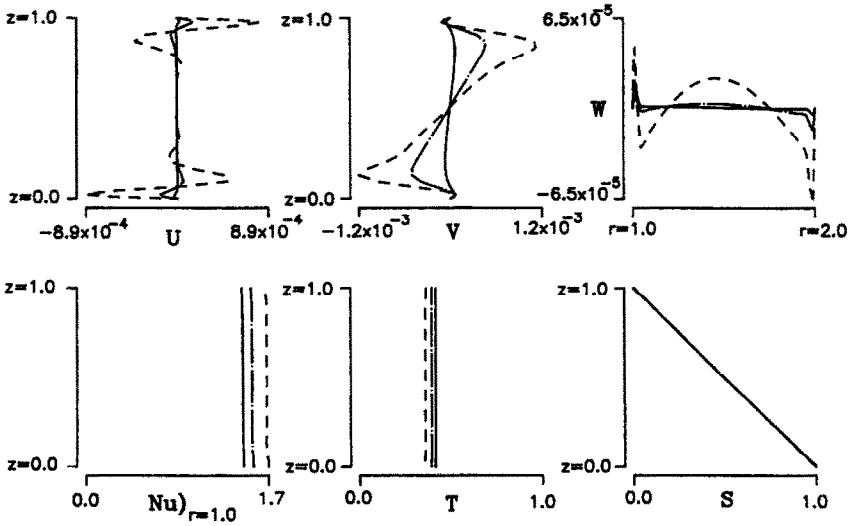

FIG. 10. Representative profiles of velocities, Nusselt number, temperature and solute. $R_\rho = 10.0$. The vertical profiles are along $r = 0.5$, and the horizontal profiles are along $z = 0.5$. ——: $St = 0.1$, — · — · — · —: $St = 1.0$, – – – –: $St = 10.0$.

qualitative character of flow, subjected to the rotation effect.

For a low buoyancy ratio, the effect of the flow-driving horizontal temperature gradient is dominant. Convection is generally vigorous, and large values of the Nusselt number are obtained. When St is small, the rotation effect is appreciable, and the convective flows weaken accordingly. When R_ρ takes a moderate value, the flow structure depends crucially on St. For a small St, the rotation effect is substantial, and the global flow field is strongly influenced by conduction. When the rotation effect is small (St large), convective activities are strengthened. For a large buoyancy ratio, the stabilizing solutal gradient suppresses convection. The resulting flows are very weak in the interior. The temperature field is horizontally linear, and the vertical solutal gradient is little affected. The heat transfer is dominated by conduction.

These computational results will provide the baseline information on the qualitative features of the axisymmetric basic states. These could be utilized to develop stability analyses for more complicated three-dimensional flows.

Acknowledgement—Appreciation is extended to the referee whose comments led to substantial improvements in the revised version.

REFERENCES

1. J. S. Turner, Double diffusive phenomena, *Ann. Rev. Fluid Mech.* **6,** 37–56 (1974).
2. H. E. Huppert and J. S. Turner, Double diffusive convection, *J. Fluid Mech.* **106,** 299–329 (1981).
3. C. F. Chen and D. H. Johnson, Double diffusive convection: a report on an engineering foundation conference, *J. Fluid Mech.* **138,** 405–416 (1984).
4. J. W. Lee and J. M. Hyun, Double-diffusive convection in a cavity under a vertical solutal gradient and a horizontal temperature gradient, *Int. J. Heat Mass Transfer* **34,** 2323–2427 (1991).
5. S. Ostrach, Natural convection with combined driving forces, *Physico-chemical Hydrodyn.* **1,** 233–247 (1980).
6. H. E. Huppert and P. F. Lindeu, On heating a stable salinity gradient from below, *J. Fluid Mech.* **95,** 431–464 (1979).
7. F. P. Incropera and R. Viskanta, Optical studies of mixed layer development in a double diffusive, thermohaline convection, *Proc. 7th Int. Heat Transfer Conf.* **2,** 419–424 (1982).
8. J. W. Lee and J. M. Hyun, Time-dependent double diffusion in a stably stratified fluid under lateral heating, *Int. J. Heat Mass Transfer* **34,** 2409–2421 (1991).
9. J. M. Hyun and H. S. Kwak, Double-diffusive convection in a cylinder with a spinning endwall disk, *Geophys. Astrophys. Fluid Dyn.* **46,** 203–219 (1989).
10. H. Ozoe and K. Kamakawa, Double-diffusive natural convection between vertical parallel walls: numerical analysis for two-layer convection, *Proc. ASME–JSME Thermal Engng Joint Conf.* **1,** 141–146 (1991).
11. O. S. Kerr and J. Y. Holyer, The effect of rotating on double-diffusive interleaving, *J. Fluid Mech.* **162,** 23–33 (1980).
12. S. R. Coriell, M. R. Cordes and W. J. Baettinger, Convective and interfacial instabilities during unidirectional solidification of a binary alloy, *J. Crystal Growth* **49,** 13–28 (1980).
13. A. J. Chorin, Numerical solution of the Navier–Stokes equations, *Math. Comput.* **22,** 745–762 (1968).
14. H. C. Ku, R. S. Hirsh and T. D. Taylor, A pseudospectral method for the solution of the three-dimensional incompressible Navier–Stokes equations, *J. Comp. Phys.* **70,** 439–462 (1987).
15. H. C. Ku, T. D. Taylor and R. S. Hirsh, Pseudospectral methods for solution of the incompressible Navier–Stokes equations, *Computers Fluids* **15,** 195–214 (1987).
16. J. W. Lee and J. M. Hyun, Double-diffusive convection in a rectangle with opposing horizontal gradients of temperature and concentration, *Int. J. Heat Mass Transfer* **33,** 1619–1632 (1990).
17. J. M. Hyun and J. W. Lee, Double-diffusive convection in a rectangle with cooperating horizontal gradients of temperature and concentration, *Int. J. Heat Mass Transfer* **33,** 1605–1618 (1990).
18. V. Barcilon and J. Pedlosky, A unified linear theory of homogeneous and stratified rotating fluids, *J. Fluid Mech.* **29,** 609–201 (1967).